Physics of the Earth and Planetary Interiors 171 (2008) 158–169

Contents lists available at ScienceDirect

Physics of the Earth and Planetary Interiors

journal homepage: www.elsevier.com/locate/pepi

Geological modelling from field data and geological knowledge Part II. Modelling validation using gravity and magnetic data inversion

A. Guillen[a,*], Ph. Calcagno[a], G. Courrioux[a], A. Joly[b], P. Ledru[a]

[a] BRGM, BP 6009, 45060 Orléans Cedex 02, France
[b] Centre for Exploration Targeting, M006, 35 Stirling Highway CRAWLEY WA 6009, Australia

ARTICLE INFO

Article history:
Received 31 October 2007
Received in revised form 24 April 2008
Accepted 11 June 2008

Keywords:
3D geology
Inverse problem
Metropolis
Potential field
Probability
Gravity
Magnetism
Tensors

ABSTRACT

The analysis of multiple data sets is required to select a realistic 3D geological model among an infinite number of possibilities. An inverse method that aims at describing the 3D geometry of geological objects is presented. The method takes into account the geology and the physical properties of rocks, while respecting the topological properties of an a priori model. The a priori model is built from the geological data set and its geometry is largely dependent upon assumptions about inaccessible geology at depth. This method, referred to as "total litho-inversion" is a generalised 3D inversion that results in quantifying the lithology and the distribution of rock property in a probabilistic way. Its application is demonstrated through (i) a simple synthetic case and (ii) the relative distribution characterization of granites and diorites in an orogenic domain.

1. Introduction

Our knowledge of the geology of the lithosphere can be summarized in term of our capacity to predict the extension of geological structures, objects and phenomena in space and time. The problem in exercising such a prediction arises from the difficulty in understanding the complexity of the geological phenomena. Our ability to progress in our knowledge of the geology therefore amounts to our capacity to model and represent the phenomena. In this respect, any method of 3D inversion applied to geological and geophysical data opens up new perspectives in terms of quantifying the geological uncertainty.

The main problem facing the geologist is the impossibility of making continuous observations in the subsurface domain except for occasional access to drill cores or underground works. In a first stage, he has to formulate depth extension hypotheses using vertical sections that may already be highly conceptual. In particular, in detail, the number of geological models that could be constructed from the surface data is infinite. To progress, the geologist is forced to use a combination of methods of indirect imagery to determine possible extensions of the geological structures and objects at depth. Each method is calibrated according to the type of data and its knowledge of variation laws; for example, the inverse problem can be successfully applied to quantify uncertainty of the petrophysical properties model (Tarantola and Valette, 1982; Li and Oldenburg, 1998). However, the interpretations specific to each method do not arrive at a single solution that would make it possible to select among the infinity of geological starting models. Although the structural representation may be correct at regional scale, the applied geological work and the problems encountered, for example in tunnel digging, exhibits the uncertainty in the constructed models (Blanchin and Chilès, 1993).

We present a programmable method referred to as 'total litho-inversion', to obtain a 3D probabilistic description of geological objects at depth taking into account the complete set of available data, i.e., geological maps, borehole data, structural data (Calcagno et al., this issue), physical properties of the rocks, geophysical measurements such as gravity and/or magnetic potential field and tensor data. This method overcomes the problem of identifying the "most probable" or the "best" model (Tarantola, 2006) through testing all possible models using a range of different geometries. It provides not only one model, but a probability distribution over the model space, thanks to its sampling.

In this paper, inversion is performed on gravity and magnetic data using the Monte Carlo sampling of solutions (Metropolis and Ulam, 1949; Metropolis et al., 1953; Mosegaard and Tarantola, 1995;

* Corresponding author. Tel.: +33 2 38 64 30 54; fax: +33 2 38 64 33 34.
E-mail address: a.guillen@brgm.fr (A. Guillen).

0031-9201/$ – see front matter © 2008 Elsevier B.V. All rights reserved.
doi:10.1016/j.pepi.2008.06.014

Bosch et al., 2001; Tarantola, 2005). The latter papers fully describe the theory.

The method is illustrated on a synthetic example as well a real case using an a priori geological model of granitic intrusions along a vertical crustal-scale fault from the French Massif Central.

2. The a priori model

The geological map provides a geo-referenced representation of the distribution of the main geological systems and units, from the 1/500,000 regional scale of the basin or mountain belt to the 1/5000 high-resolution scale showing the lateral changes of composition of a single lithologic unit. The challenge of 3D modelling rests on the difficulty of extrapolating at depth surface and exceptionally in situ observations, using appropriate interpolation algorithms and meshing. In all cases, the geological unit will constitute the elementary cell of the model and is defined by independent parameters:

- *Nature*: the lithology, defined by the mineralogical composition, is generally the basic notion that defines the nature of the unit; age of the formation or of the transformation of the rock may also characterize the unit.
- *Topology*: a geological unit must be defined in terms of its relationships with all surrounding geological units; common types of topological relationships are superposition and unconformity in basins, cross-cutting relations in volcanic and magmatic domains, superposition and truncature in metamorphic terrains; rules for building the 3D geometrical models must be formulated and integrated in the process.
- *Shape*: the size, boundaries and orientation defines the shape of the unit; the 3D geometric modelling of the shape is the key component of the 3D process referring to the *x*, *y*, *z* extent of the unit, position of the contacts between all surrounding units, orientation of internal structures.
- *Intrinsic properties*: there is an implicit relation between the nature of the geological unit and physical parameters such as density, susceptibility, magnetization, porosity, thermal conductivity, radioactivity; thus, the 3D geometrical model can be used to compute a 3D petrophysical properties model.

The knowledge of the nature of the geological units, their shape and topology generally fall in the field of expertise of the earth scientist. Thus, the 3D geometrical model will be first constrained by the information available on the geological map completed by direct field observations, drilling and/or underground works, and remote observation from space, airborne and field geophysical surveys. On the basis of this information and according to current conceptual geological models, the geologist will then resolve some indetermination of the extrapolation process by introducing interpretative cross-sections and rejecting the models that are not geologically meaningful. An original method to reach this goal is described in Calcagno et al. (this issue). At this stage, the quality of the resulting a priori model will be largely dependent on the quality, accuracy and density of data that will be integrated together with the know-how of the geologist.

Considering intrinsic properties such as density, magnetic susceptibility and remanent magnetization, their parameters can be assigned to each geological unit and the computed 3D geometric model effects can be compared to the corresponding measured potential fields. Starting from the a priori model, direct and inverse modelling can thus generate a very large number of models that will satisfy the gravity and magnetic fields and tensors of these fields.

3. Gravity, magnetic field and tensor data

The method is applied to gravity and magnetic data, with or without remanence, as well as gravity or magnetic field gradient tensor data. Gradient measurements improve accuracy and spatial resolution of gravity and magnetic surveys. The full gradiometric tensor is now measured in the oil and gas or mining prospecting. The ESA GOCE gradiometry (Gravity Field and Steady-State Ocean Circulation Explorer) will open up a whole range of new possibilities for solid Earth physics (Drinkwater et al., 2003).

Since the use of gravity and magnetic field data is well known, the following explanation will focus on the tensor data. Historically Loránd Eötvös's torsion balance allowed the first successful gravity gradiometric measurements to be made at the surface of the earth. The torsion balance was one of the earliest geophysical instruments used in the exploration for salt domes along the Texas Gulf Coast. There is increasing interest in measuring gravity gradients of the earth's gravity field. For gravity undoubtedly an advantage of these gradient measurements is their relative insensitivity to small platform accelerations which constitutes a principal problem for aerial gravimetry.

This paper will illustrate the problem focusing on the gravity tensor (Pedersen and Rasmussen, 1990); the generalisation for magnetic tensor is straightforward.

The gravity field from an extended body is most easily understood in terms of its gravity scalar potential U at the position r:

$$U(r) = G \iiint \frac{\rho(r')}{|r' - r|}\, \mathrm{d}(r'),$$

where $\rho(r')$ is the density of material at position $r'$and $G = 6.668 \times 10^{-11}\,\mathrm{N\,m^2\,kg^{-2}}$ is the gravitational constant. Gravity field and gravity gradients are easily calculated from the scalar potential and in Cartesian coordinates:

$$\mathbf{g}(r) = \mathrm{grad}(U(r)) = \frac{\delta U}{\delta x}\mathbf{i} + \frac{\delta U}{\delta y}\mathbf{j} + \frac{\delta U}{\delta z}\mathbf{k}$$

The gravity gradient is used to describe how a particular component of gravity varies with position, e.g., for the x component we have

$$\begin{aligned} g_x(r + \delta r) &= g_x(r) + \frac{\delta^2 U}{\delta x^2}\,\mathrm{d}x + \frac{\delta^2 U}{\delta x \delta y}\,\mathrm{d}y + \frac{\delta^2 U}{\delta x \delta z}\,\mathrm{d}z \\ &= g_x(r) + Exx\,\mathrm{d}x + Exy\,\mathrm{d}y + Exz\,\mathrm{d}z \end{aligned}$$

The gravity tensor

$$\mathrm{grad}(\mathbf{g}(r)) = \mathbf{E}\begin{bmatrix}\mathbf{i}\\ \mathbf{j}\\ \mathbf{k}\end{bmatrix} = \begin{bmatrix} Exx & Exy & Exz \\ Eyx & Eyy & Eyz \\ Ezx & Ezy & Ezz \end{bmatrix}\begin{bmatrix}\mathbf{i}\\ \mathbf{j}\\ \mathbf{k}\end{bmatrix}$$

$$= \begin{bmatrix} \frac{\delta^2 U}{\delta x^2} & \frac{\delta^2 U}{\delta x \delta y} & \frac{\delta^2 U}{\delta x \delta z} \\ \frac{\delta^2 U}{\delta y \delta x} & \frac{\delta^2 U}{\delta y^2} & \frac{\delta^2 U}{\delta y \delta z} \\ \frac{\delta^2 U}{\delta z \delta x} & \frac{\delta^2 U}{\delta z \delta y} & \frac{\delta^2 U}{\delta z^2} \end{bmatrix}\begin{bmatrix}\mathbf{i}\\ \mathbf{j}\\ \mathbf{k}\end{bmatrix}$$

The tensor is symmetric since the order of differentiation is irrelevant. By virtue of Laplace's equation, $Exx + Eyy + Ezz = 0$, so the number of independent components reduces to five. The values of the components depend upon the choice of the axes. Here x is assumed towards the East, y is towards the North and z is up.

For a spherical body of mass M with radial density function spherical polar coordinates give

$$U(r) = \frac{GM}{r}, \quad g(r) = -\frac{GM}{r^2}, \quad \mathrm{Err} = \frac{2GM}{r^3},$$

where r refers to distance from centre. Other components can easily be calculated and other coordinate systems can be used; the main point to note here is that the gravity gradient has a more rapid variation with position than does gravity and so falls away quicker from its maximum value near a mass anomaly. This ultimately translates to gravity gradient providing better estimation of edge location than does gravity.

For the magnetic tensor we can generalise the previous formulation starting from the Poisson relation for a body with uniform susceptibility k and uniform polarization $\mathbf{I} = k\mathbf{H}$, where $\mathbf{H}$ represents the magnetic field we can relate magnetic potential to gravity potential for bodies of same shape and size, i.e., magnetic potential (and hence magnetic field) can be found from gravitational potential for body (sphere, cylinder, polygon, etc.), using Poisson relation we obtain

$$U_{\mathrm{mag}}(r) = \frac{I}{G\rho}\frac{\delta U_{\mathrm{grav}}(r)}{\delta i},$$

where i is the direction of uniform polarization $\mathbf{I}$.

It is well known that the inverse problem in potential field methods is ill-posed (Laplace's equation has an infinity of solutions). What is the advantage of using tensor data for the inverse problem? Using tensor will naturally not fully resolve the non-uniqueness; it will shrink the space of solutions. In summary, the tensor defines the shallow structures, while the gravity/magnetic field has less possibility to define these last ones but defines the deep structures.

4. Forward modelling

We base forward modelling and inversion on a voxel (a volume element) representation of the model. The geological model will be investigated as an assembly of homogeneous voxels with adjustable density contrast. For each voxel, the appropriate stratigraphic unit is assigned, based on the geological model. The specially prepared potential field data set dictates the (x, y) dimensions of the voxels; the z discretisation is typically set to the same value throughout, though may be reduced for finer discretisation. Analytical expressions (Plouff, 1976; Okabe, 1979; Holstein, 2003) are used to compute the gravity or magnetic field and the corresponding tensor effect of these voxels.

5. The inversion strategy

The geological model is discretised into a 3D matrix of cells (voxels) in order to produce an initial 'lithology' model. Lithology, a categorical variable (i.e., one that acts as a label rather than as a numerical value), is the primary model parameter. The present implementation holds the lithology of surface voxels fixed throughout the inversion. The lithology associated with subsurface voxels is free to vary, subject to the condition that the topology of the initial model remains unchanged. The inversion explores variations to the initial model which reproduce the supplied gravity or magnetic data within a desired tolerance level. The adopted strategy is to randomly walk around the space of possible models for a given set of a priori information. This approach was proposed by Mosegaard and Tarantola (1995) and developed in 2D by Bosch et al. (2001).

Many transient models are derived from the a priori model using an iterative procedure, with two possible updates. The physical property, density or induced magnetization and remanent magnetization, for a randomly selected voxel that is separated from the boundary of that unit, may be modified. Alternatively, the lithology of a voxel that lies on the interface between two or more units may be modified, and a new physical property may be assigned to that voxel according to a random selection from the probability density function (pdf) of the relevant physical property. The voxels to which the latter operation can be applied is restricted by the constraint that the topology of the model not be altered.

The change in the misfit between the observed gravity and/or magnetic field and tensor components data and the responses calculated for the modified model is determined. This change is examined in a probabilistic framework to determine whether the modification to the model is accepted.

6. Detailed outline of the inversion algorithm

The 12 steps of the algorithm that allow us to sample the a posteriori model by inverting geophysical data such as gravity and magnetic (field and/or tensor components), are

1. Build the a priori model
   An a priori model is built, for a given hypothesis, to obtain the starting model (m_0). This model is constrained by a set of data (pc_0) that is not modifiable, and by a set of hypothetical data (p_0) that can be modified as long as the change does not alter the topology of the model. The construction of this model provides a topology (BRep: Boundary Representation) for volume elements, where each volume element V_j represents a formation j of the current a priori model hypothesis.
2. Discretize this model
   The study zone is subdivided with a matrix 3D of cells spaced at intervals of Δ_x, Δ_y, Δ_z along axes x, y, z, and each cells is assigned with the colour of the containing volume. The choice of intervals Δ_x, Δ_y, Δ_z controls the effective disturbance.
   The result is a set of cells C that are constrained by the following conditions:
   - The lithology represented by the cells containing $\{pc_0\}$ cannot be modified.
   - The lithology represented by the other cells can be modified.
3. Map the topology
   The spatial network relationships (topology) defining connections between homogeneous rock unit regions are mapped from the geological model to the voxel model. The topology must remain unchanged throughout the inversion.
4. Make a list of the boundaries or frontier cells
   The boundary or frontier cells need to be identified and updated during the inversion. The lithology parameter of a frontier cell may be changed during the inversion provided this does not alter the topology of the model. This allows the boundaries to migrate during the inversion.
5. Define the a priori probability density function (pdf) for each petrophysical parameters and for each formation or lithology
   For example, the density of a formation F_i could be represented by a normal or log-normal law $f(\log(d_i)) = N(\bar{d}_i, \sigma_i)$, where $\bar{d}_i$ represents the mean and σ_i the standard deviation in the probability density function (pdf). The choice of the a priori pdf for each petrophysical parameter for each formation or lithology is a key point (Bosch et al., 2001). This function must be defined using statistics on petrophysical measurements when they are available.
6. Compute the elementary gravity or magnetic effect (field and/or tensor's components) for each cell
   For each field or tensor component involved in the inversion process and for each cell obtained from the discretization of the

starting model, the elementary effect (field and tensor) using a unit physical property value is computed.

7. Sample the density or magnetization parameter for the set of cells C and initialize the likelihood of the model

   Sampling (Stadlober and Zechner, 1999) the parameter (e.g., density, induced and remanent magnetization) for the set of cells C is carried out according to Step 5. The gravity or magnetic (field or tensor) effects of the standard model are computed, subject to formation of the cells.

   The likelihood $L_j(m_{cur}) = k\exp(-S_j(m_{cur})/\sigma j^2)$ of the current model m_{cur}, for the geophysical field j relies on the following terms:

   - $S_j(m_{cur})$, which represents the misfit with geophysical field j, for example

     $$S_j(m_{cur}) = \frac{1}{2}\sum_{l=1}^{N}(g_j^l(m_{cur}) - \text{data}_j^l)^2;$$

     i. $g_j^l(m_{cur})$, which represents the total effect for the geophysical field j of the model at the point of observation l while data_j^l represents the measurement of the field at the same point;
   - σ_j^2, which represents the variance of the data for the geophysical field j. In general, it is assumed that σ_j^2 is identical for all the measurement data.
   - k is a normalisation factor.

   Here, we have use the L_2 norm, but the L_1 or L_∞ norms could be used.
8. Start the inversion process
9. Disturb the model m_{cur}

   The model m_{cur} is disturbed according to the following sequence:
   - Either a modification of the petrophysical parameters or a modification of the geometry (re-allocation of a cell to another formation) is made.
   - If there is modification of the geometry, then work on the frontier
     - o Choose a cell from the list of frontier cells with an equiprobable random sampling method. The selected cell is C_m.
     - o For the cell C_m not included in $\{pc_0\}$, identify and list all the formations. Then randomly sample this list to choose a formation by an equiprobable random sampling method. If there are n different formations the probability of having a formation is $1/n$. If F_i is the selected formation, assign this formation to the cell C_m. At the same time, sample the parameter (in this case density or magnetization), as defined in Step 5.
     - o To compute the geophysical disturbance brought to the model, recompute the effect of the disturbed cells.
   - If there is a modification to the petrophysical parameters, then work inside the formations
     - o Choose a cell from the list of cells that are completely included in a formation using an equiprobable random sampling method. The selected cell is C_m.
     - o Sample the parameter (in this case density or magnetization) as defined in Step 5.
     - o Compute the geophysical disturbance caused by the model. This involves recomputing the effect of the disturbed cells.

   Increment n is the number realized by the inversion process. The new disturbed model is named m_{pert}.

   The next section discusses other operations realized to modify the geometry of the model, using morphological operations.
10. Compute the geophysical effects of the model

    The geophysical effects of the model are computed summing the effects, for each geophysical field j, for the set of cells C.
11. Compute the likelihoods of the model $L_j(m_{pert}) = k\exp(-S_j(m_{pert})/\sigma_j^2)$ for each field j
    - Loop on each field j:
      - o Compute $L_j(m_{pert})$.
      - o If $L_j(m_{pert}) > L_j(m_{cur})$ then keep the disturbed model.
      - o If $L_j(m_{pert}) \le L_j(m_{cur})$ then keep the disturbed model with random sampling and a probability equal to $L_j(m_{pert})/L_j(m_{cur})$.
      - o If m_{pert} is rejected for this field, stop the loop.
    - End of the loop

    At the end of the previous loop, if m_{pert} is kept, set $m_{cur} = m_{pert}$. If not, m_{cur} is not modified.

    As we are within the scope of optimization of convex functions, classical algorithms (conjugate gradient, Newton, etc.) are of no use because they would return only one local minimum, whereas we are looking for a good representation of the space model. We have to avoid the iterations values becoming concentrated in a trough. This means sometimes accepting models that will raise the convergence threshold (i.e., we deliberately deteriorate our 3D model) to reach a new trough and compute a new set of possible models. Fig. 1 gives an example of the evolution of the likelihood function $L_j(m)$ and clearly illustrates this mechanism—during the initial part of the inversion, the data misfit for each field of the current model follows a generally decreasing trend. At some point, the data misfit reaches an asymptotic value and we begin to store the models (see Fig. 1).

    This process is an original contribution to the algorithm. To explore the space of the models we need to keep the current model and let the likelihood function $L_j(m)$ increase.

    These stored models are an exploration of the probability space of acceptable models.
12. Return to Step 10 and repeat the process

    After completing Step 11, the inversion returns to Step 10 and continues to iterate around this loop. An ensemble of models that can satisfactorily explain the geophysical signature might be explored by continuing for a further million iterations.

    Following inversion, the set of acceptable models is examined. The probability of finding any particular unit in 3D space is computable from the models stored. The most probable model could be also computed, as in each voxel we can put the geological unit with the highest probability. For gravity and magnetic data, for example, we can also compute the mean density or magnetizations for each voxel and the associated standard deviation.

7. Disturb the model: erosion, dilation, opening, closing

7.1. Preservation of an acceptable geometry

From the convergence point of view, the Metropolis algorithm is designed to obtain geophysical effects in the final models that are close to the measured effect. Unfortunately the geological contents of the 3D models can lose their consistency, with various geologi-

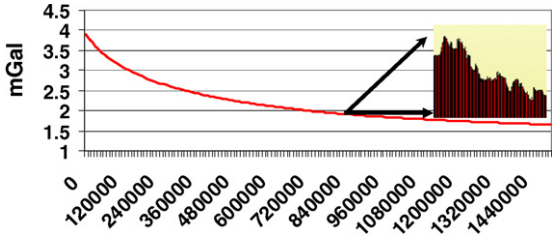

Fig. 1. Evolution of the likelihood, showing that in some areas it can increase to explore the space model.

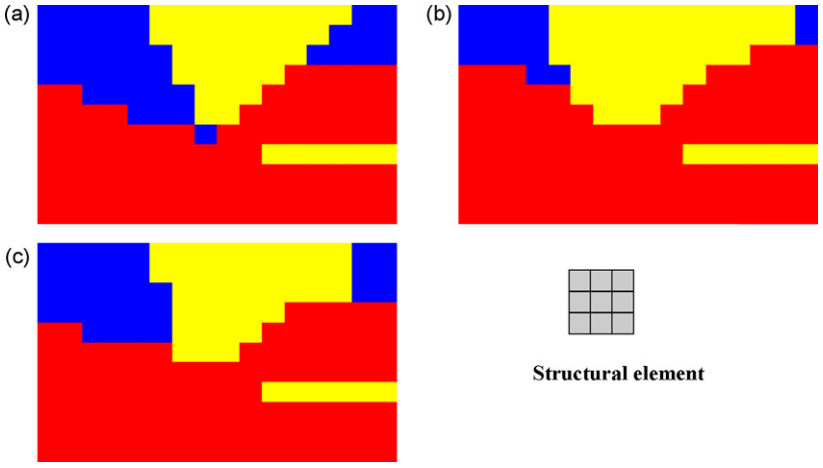

Fig. 2. (a) The geological model. (b) Same model after an erosion of the blue unit. (c) Dilation applied to (b), which represents an opening on blue unit of the original model in (a).

cal layers losing their homogeneity and their cells being scattered. The method is able to optimize a mathematical criterion effectively, but fails to guarantee that the model obtained will be geologically acceptable. For this reason, during the inversion process, at Step 9, after some iterations a morphology-based operation is applied to homogenise the current model (Serra, 1982, 1988). Erosion, dilation and their combinations are used to:

- add or remove voxels from the boundaries of features in order to smooth them;
- join separated portions of features or separate touching features;
- remove isolated voxels, representing noise, from the model.

Dilation turns voxels "on" according to rules based on the number or arrangement of neighbouring voxels; erosion turns pixels "off" according to similar rules, while Opening – an erosion followed by a dilation – and Closing – the reverse sequence – attempt to restore the original features but with some rearrangement of the boundary pixels. These operations will control the "quality" of the model.

7.2. Definitions

The object **A** consists of those voxels v that share some common property. In our case, **A** is the set of voxels which are in the same geological unit:

Object $\mathbf{A} = \{v|\text{property}(v) == \textbf{TRUE}\}$

The background of **A** is given by $\mathbf{A}^c$ (the complement of **A**) which is defined as those elements that are not in **A**:

Background : $\mathbf{A}^c = \{v|v \notin \mathbf{A}\}$

We will define quickly the fundamental operations associated with an object in mathematical morphology. The standard set operations are union, intersection, and complement plus translation:

Translation—given a vector **x** and an object **A**, the translation $\mathbf{A}+\mathbf{x}$ is defined as

$$\mathbf{A} + \mathbf{x} = \{v + \mathbf{x}|v \in A\}$$

The basic Minkowski set operations – addition and subtraction – can now be defined. Given two objects **A** and **B**:

Minkowski addition

$$\mathbf{A} \oplus \mathbf{B} = \bigcup_{\beta \in \mathbf{B}} (\mathbf{A} + \beta)$$

Minkowski subtraction

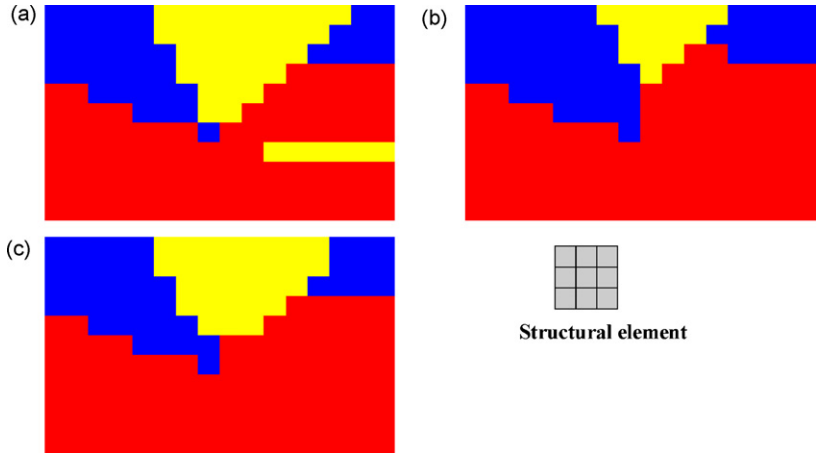

Fig. 3. (a) The geological model. (b) Same model after an erosion of the yellow unit. (c) Dilation applied to (b), which represent an opening on yellow unit of the original model in (a).

$$\mathbf{A}\Theta\mathbf{B} = \bigcap_{\beta\in\mathbf{B}} (\mathbf{A}+\beta)$$

7.3. Dilation and erosion

From these two Minkowski operations we define the fundamental mathematical morphology operations dilation and erosion:

Dilation

$$D(\mathbf{A},\mathbf{B}) = \mathbf{A}\oplus\mathbf{B} = \bigcup_{\beta\in\mathbf{B}} (\mathbf{A}+\beta)$$

Erosion

$$E(\mathbf{A},\mathbf{B}) = \mathbf{A}\Theta(-\mathbf{B}) = \bigcap_{\beta\in\mathbf{B}} (\mathbf{A}-\beta)$$

where

$$-\mathbf{B} = \{-\beta | \beta\in\mathbf{B}\}$$

A is usually considered as an "image" and **B** is called a structuring element. The structuring element is to mathematical morphology what the convolution kernel is to linear filter theory.

Dilation and erosion share the main properties (associative, translation invariance and duality).

7.4. Opening and closing

We can combine dilation and erosion to build two important higher order operations: opening and closing.

Opening

$$O(\mathbf{A},\mathbf{B}) = \mathbf{A}\circ\mathbf{B} = D(E(\mathbf{A},\mathbf{B}),\mathbf{B})$$

Closing

$$C(\mathbf{A},\mathbf{B}) = \mathbf{A}\bullet\mathbf{B} = E(D(\mathbf{A},\mathbf{B}),\mathbf{B})$$

The opening and closing operations also have many properties. The opening operation can separate geological unit that are connected with an isthmus. The closing operation can fill in small holes. Both operations generate a certain amount of smoothing on an object contour, given a "smooth" structuring element. The opening smoothes from the inside of the object contour while the closing smoothes from the outside of the object contour.

7.5. Examples

These operations are illustrated in Figs. 2 and 3 on 2D examples; the extension to 3D is straightforward. When erosion is applied, the eroded voxel will be assigned to a geological unit randomly selected in the set of units present in the structural element.

The process of opening, on the blue unit, is illustrated Fig. 2 with three geological units and a structural element with a size of 3×3. In Fig. 3, the opening operation is applied on the yellow unit, which makes the yellow band included in the red unit disappear.

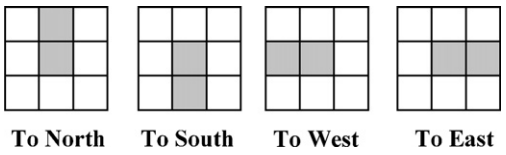

Fig. 4. 2D structural element use for directional growing/thinning.

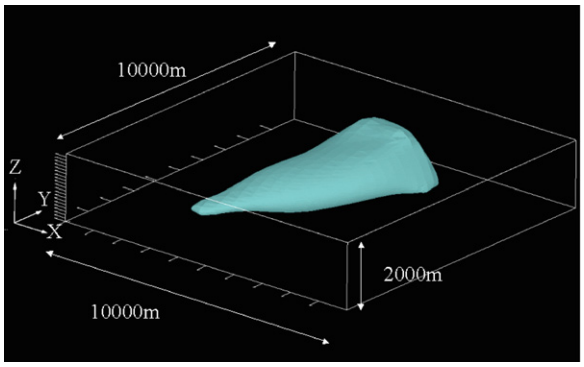

Fig. 5. South-East view of the synthetic 3D model.

7.6. Growing and shrinking geological units

The previous method allows modifying the shape of the geological units using growing (dilation process) or shrinking (erosion process). This operation occurs during Step 9 of the inversion process. After a random number of iterations, a geological unit is randomly selected. For this unit an operation (growing or shrinking) is randomly selected as well as one of the six possible directions (to North, to South, to East, to West, to Top, to Bottom). Fig. 4 illustrates the different 2D structural elements used with dilation and erosion to obtain growing or shrinking of the shapes in the different directions.

8. Synthetic example

The method is tested on a synthetic case assumed to represent the sought after reality. The geological model is represented in Figs. 5 and 6. The body has a constant contrast of volumetric mass equal to 1000 kg/m^3, the top of the body is at 260 m depth, and the bottom is 2000 m depth. For this body the gravity effect and the tensor are shown in Fig. 7.

The main point to note here is that the gravity gradient clearly defines the top of the structure and its main NE–SW orienta-

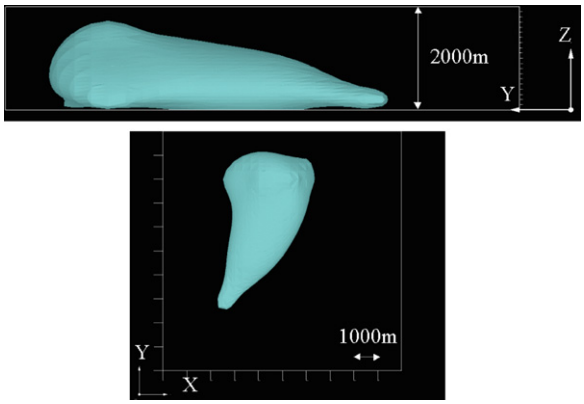

Fig. 6. Different points of view of the synthetic 3D model. On the upper part: view from the west. On the lower part: view from the top.

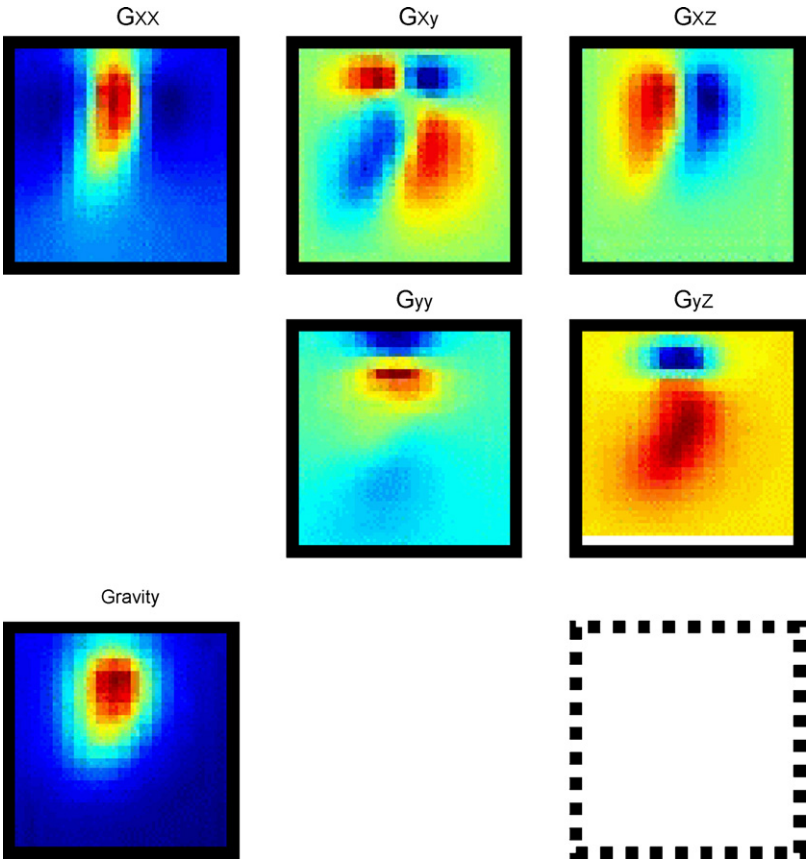

Fig. 7. Tensor components and gravity effect of the synthetic 3D model. The *Gzz* component is not represented since equal to $-(Gxx + Gyy)$.

tion. The gravity field displays the same feature but with less contrast.

The inversion method is tested with an a priori model, simpler than the synthetic one (Fig. 8). This model is smaller and shallower, with a N–S orientation. The starting tensor and gravity field effect are shown in Fig. 9.

The starting gravity field and gravity tensor are computed assuming the volumetric mass property contrast according to a Gaussian distribution with mean equal to 1000 kg/m^3 and standard deviation equal to 200 kg/m^3. The standard deviation error on the measurements is 3 μm s^{-2} for the gravity field and 3 E.U. (10^{-9} s^{-2}) for each tensor component. The result after 100,000 iterations is shown in Fig. 9.

Fig. 10 shows the comparison along a SW–NE cross-section with the "real model in (a) and the results of the inversion in (b) and (c). In (b) we have the probability to obtain the body using only gravity field inversion. In (c) we have the probability to obtain the body with gravity field inversion plus the inversion of the five components tensor. In (b) and (c) the red lines represent the a priori model shown in 3D in the previous figures. Using tensor data, the results show closer agreement to the synthetic model in the northern, the south-western and bottom parts. In both cases results can be qualified as acceptable. However, the quality of the results increases using simultaneous inversion of independent fields.

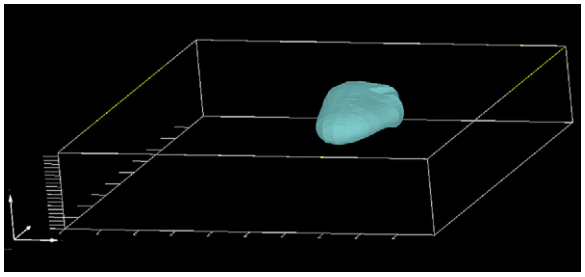

Fig. 8. Starting model for inversion, viewed from the South.

9. Application to a case history: modelling of granitic intrusions along a vertical crustal-scale fault from the French Massif Central

9.1. Geological context

Granite generation and emplacement during orogenesis is a widespread phenomenon that remains debated in terms of mechanism of ascent and intrusion. Thus, the drain role of the vertical fault system is often invoked to justify the transfer of large amounts of granitic melt from the middle crust towards upper levels. Such situation has been studied in the case of the Montmarault plutonic complex that is situated in the northern part of the French Massif Central (Joly, 2007; Joly et al., 2008). Several bodies, with different gravimetric and magnetic properties, are aligned on the Western side of a sub-vertical crustal-scale fault system that extends over more than 500 km from North to South, the Sillon Houiller Fault (SHF). Mapping, lithological and mineralogical studies, U–Th/Pb dating, field structural observation and magnetic susceptibility anisotropy studies, have shown that the Montmarault plutonic complex emplaced within host metamorphic series during the Namurian at about 320 Ma. The intrusion is controlled by a regional NW–SE maximum stretching direction, also recorded by other

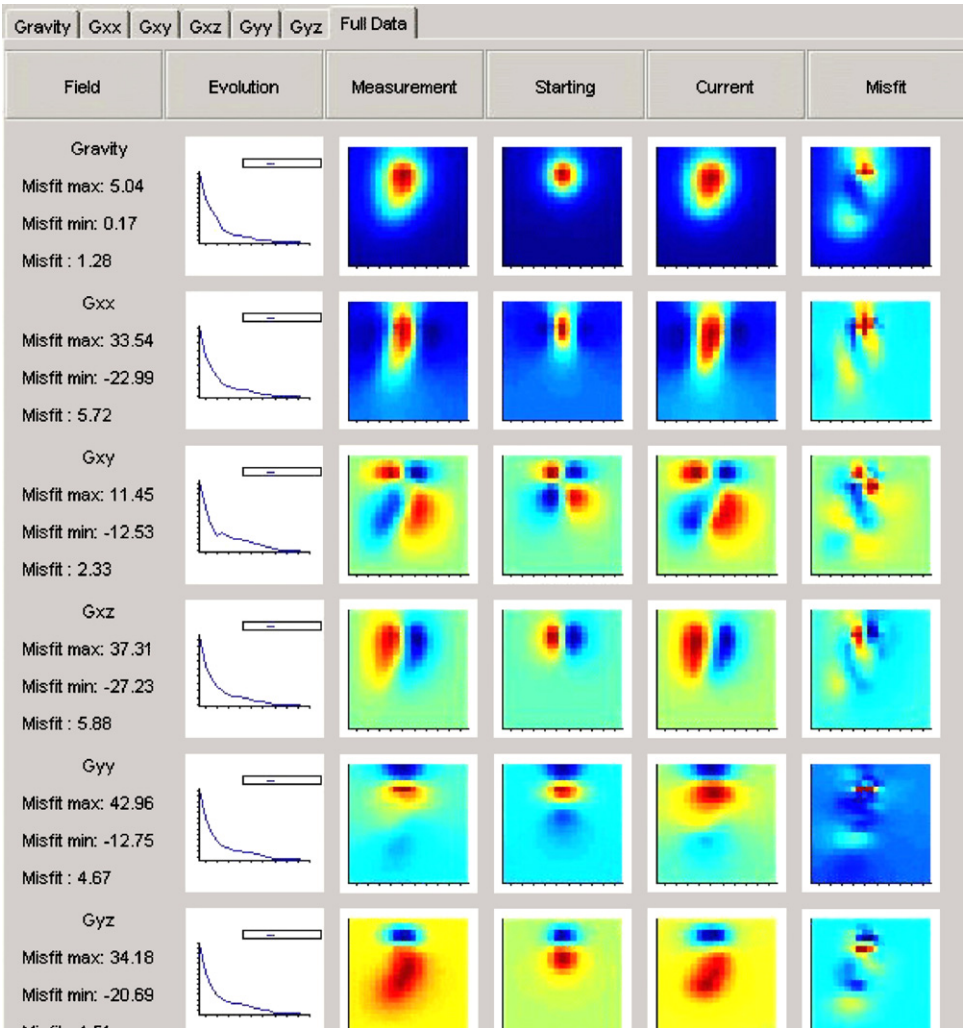

Fig. 9. State of the fields after 100,000 iterations in the inversion process. From the left to the right for each component we have a description of the misfit, the measured component, the component for the a priori model, the component of the current model and the misfit.

Namurian granites throughout the French Massif Central (Faure, 1995). An a priori geometrical model has been built using all available mapping information (Fig. 11). This initial model is of interest in terms of regional geology, however it is unconstrained concerning the relationship between granitic intrusion and crustal-scale fault. Therefore the total litho-inversion of gravity and magnetic fields has been applied to the a priori model in order to evaluate the possible rooting of the intrusions and the role of the fault system.

As shown by Bouguer anomaly and magnetic maps (Fig. 12), the important negative gravity and magnetic anomalies are well located along the SHF and since correlated to the thickening of the granite in the vicinity of the fault system. To the west of the SHF, the important positive V-shaped magnetic and gravity anomalies suggest that a thin granite of laccolithic shape, is probably underlain by intrusions of diorite with high magnetic susceptibility and density locally outcropping as pods. The late Paleozoic sedimentary basins correspond to half-graben structures, characterized by both negative gravity and magnetic anomalies.

9.2. A priori model

The a priori model contains 30 geological units and faults. The granitic complex is divided in three units, with different lithologies and contrasted magnetic properties. Petrophysical properties of the modelled units are indicated in Table 1, the probability distribution for both density and susceptibility is modelled from measurements as a log-normal law.

Model is a parallelepiped 64 km long, 58 km wide and 4 km deep. It was discretized using a grid of $64 \times 58 \times 20$ parallelepipeds, which results in 74,240 parallelepipeds of $1000\,\text{m} \times 1000\,\text{m} \times 200\,\text{m}$.

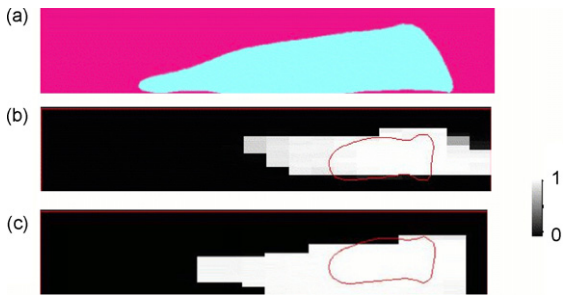

Fig. 10. Comparison between the synthetic model and inversion results. (a) Synthetic model. (b) Probability to obtain the unit after inversion of the gravity field only. (c) Probability to obtain the unit after simultaneous inversion of the gravity field and the five tensors components.

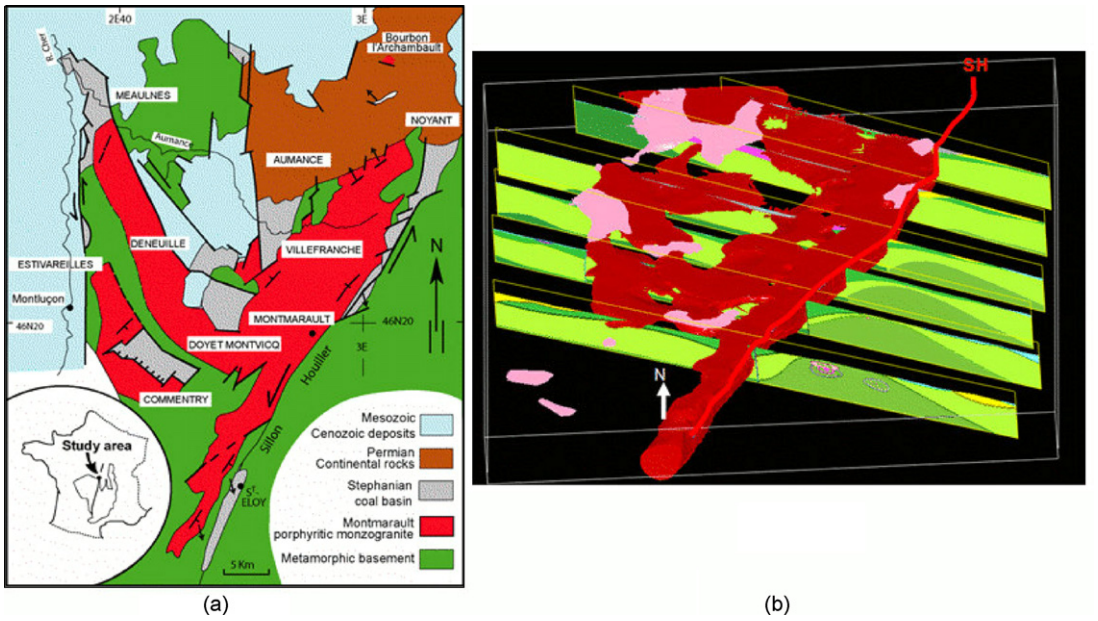

Fig. 11. A priori model for inversion. (a) Geological map of the studied area. (b) South-East view of the 3D a priori model generated using maps and orientations foliations. The 3D geometry of metamorphic units is displayed only on cross-sections perpendicular to the Sillon Houiller Fault (SH), whereas granites and leucogranites are displayed in full 3D respectively in red and pink. The SH is the East limit of the granites.

9.3. Litho-inversion

For the results described here, the litho-inversion of the model involved 4 h of computation with 1,000,000 iterations, of which 56% resulted in modifications to the model, and 44% were rejected. Among the modifications, 45% concerned the boundaries and 55% were inside the formations. The grids used to perform the inversion are built from different surveys; empirically the error on measurements assigned to the gravity data is 8 $\mu m\,s^{-2}$ and 5 nT for the magnetic data.

The a priori model, obtained by applying the discretization algorithm as described above, represents the hypothesis accepted by the geologist (Fig. 11). From this model, the total litho-inversion method provides a set of 560,000 of different models explaining both gravity and magnetic anomalies, taking into in account the petrophysical data (densities, susceptibilities and no remanent magnetization in this case). Fig. 12 shows the agreement between the fields created by the model and the measurements, just after 330,000 iterations. Each of them gives a particular model that is saved in the computer's memory in order to study statistically the space of solutions visited by the total litho-inversion method. This data structure shows the probabilities of a given lithology at any 3D location of the underground and provides a genuine scanner of the continental crust. It is thus possible to visualize laterally and in

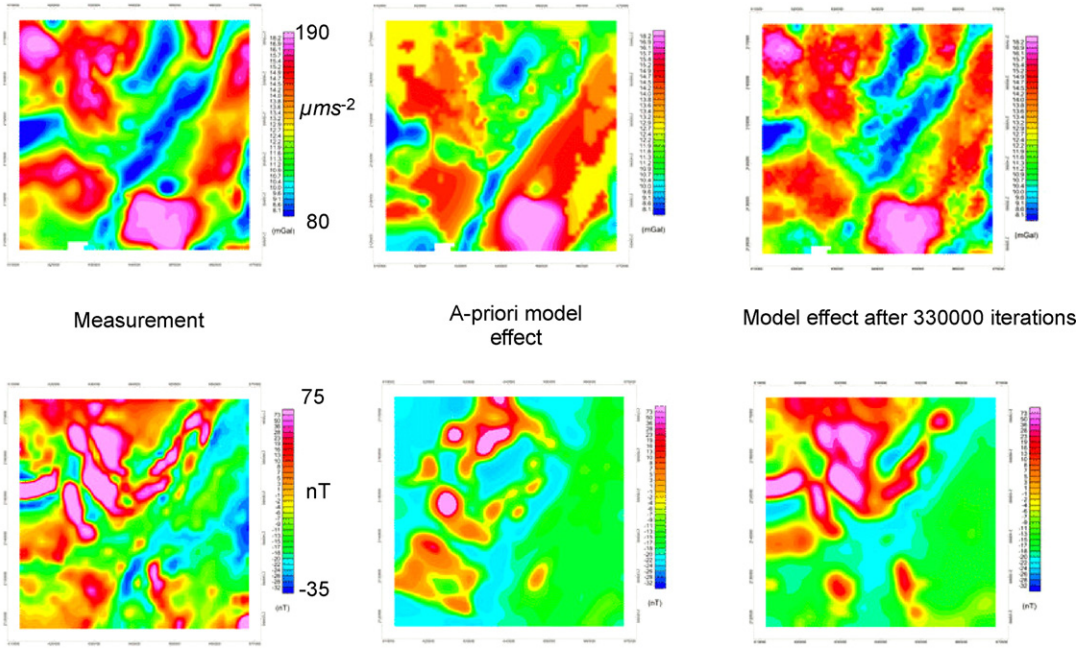

Fig. 12. Gravity and magnetic anomalies used for inversion. On the upper part: gravity fields, on the lower part: magnetic fields. From left to right: measurements, a priori model effect and model effect after 330,000 iterations.

Table 1
Petrophysical properties of the modelled units

Units		Density kg/m^3	Density variation kg/m^3	Susceptibility μSI	Susceptibility variation μSI
Mesozoic and Cenozoic deposits		2500	80	13	6
Permian basin		2500	30	25	13
Stephanian basin		2540	30	25	13
Leucogranite Sioule		2670	20	3142	628
Servant unit		2620	20	1257	700
Treban unit		2620	20	2513	440
Diorite Sioule		2750	20	15080	10000
Diorite 1		2840	40	1256	157
Migmatite Sioule		2750	20	1885	400
Gneiss Sioule		2750	40	628	63
East unit SH		2750	40	650	65
Leucogranite		2670	20	3142	650
Porphyritic granite 1		2670	20	13200	6000
Porphyritic granite 2		2670	20	6283	3000
Porphyritic granite 3		2670	20	126	126
Granite		2600	20	2513	500
Diorite 2		2750	50	15080	10000
Migmatite		2750	20	1885	400
Gneiss		2750	50	650	100
Micaschist		2750	20	650	100

depth the extension of the geological units by successive screening 2D images representing the probabilities of presence of a studied lithotype in a cross-section (Fig. 13).

In the case of the Montmarault plutonic complex, it can be shown that a vertical rooting of the intrusion along the Sillon Houiller fault system is supported by the litho-inversion of the gravimetric and magnetic fields.

At the scale of the studied area, a vertical rooting of the intrusion along the Sillon Houiller fault system is supported by the result of litho-inversion as granites are visible from b to e cross-sections (Fig. 13), depth of the main body increasing southwards. This modelling provides to the geologist absolutely new information to constrain the interpretation of the relationships between granite intrusions and vertical fault system. While the geologic map and a priori model suggest a widespread distribution of granites near surface, modelling reveals a high probability for the presence of large bodies at depth in the vicinity of the fault. At the scale of an individual massif, in section b (Fig. 13), the result of total litho-inversion confirms the laccolithic shape of the granite intrusion. However, a larger development of the diorite at depth is suggested, corresponding to a large magnetic anomaly. Moreover, the screening also reveals a strong contrast between the lithologies at depth on each side of the fault system, suggesting a role of vertical frontier for the Sillon Houiller fault. The structures are thus clarified from the standpoint of volume and position, and the a posteriori density and susceptibility distributions, globally confirm the hypotheses on the density and magnetization values (Fig. 14).

In conclusion, we confirm that the geological hypothesis used to build the geological model and the petrophysical measurements are compatible with the geophysical measurements of the gravity and magnetic fields. New constrains are drawn for the role of the Sillon Houiller fault system as a major drain controlling the ascent of the granitic intrusions and as a frontier separating two crustal blocks of different bulk composition. More than of regional interest, this case history is considered as representative of many geologi-

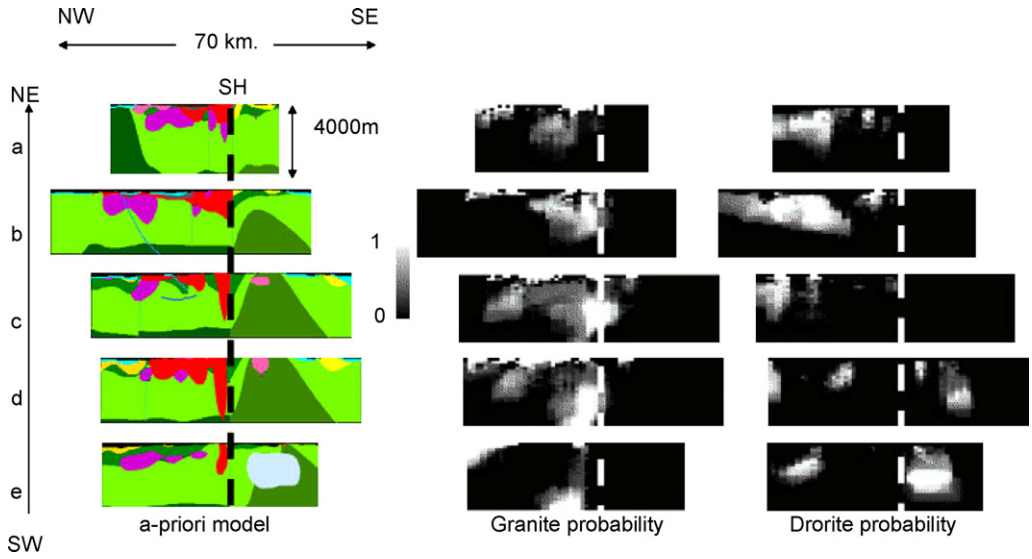

Fig. 13. Cross-section screening through the 3D models from South-West to North-East with NW–SE cross-sections. The cross-sections are aligned on the Sillon Houiller Fault (SH). From left to right: the a priori model, the probability (in white probability is equal to 1, in black probability is equal to 0) to have granites and leucogranites, and the probability to found the diorites.

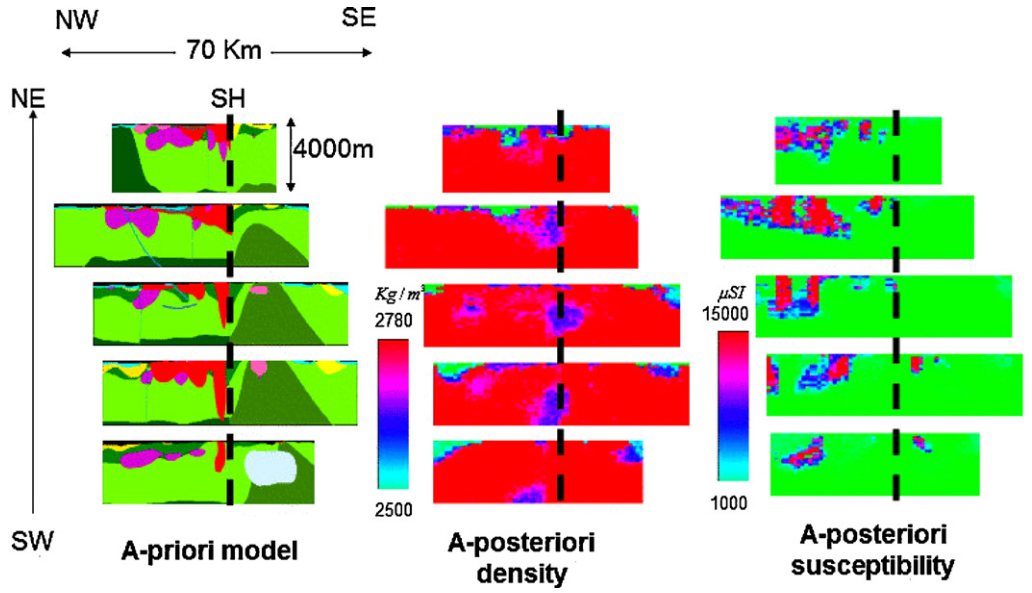

Fig. 14. Cross-section screening through the 3D models from South-West to North-East with NW–SE cross-sections. The cross-sections are aligned on the Sillon Houiller Fault (SH). From left to right: the a priori model, mean density and the mean susceptibility (we have just an induced magnetization).

cal contexts within different orogens. Such study could be of great interest to evaluate the coupling between tectonic processes and granite generation and emplacement.

10. Conclusion

The method shows that a probabilistic description of subsurface lithologic structures can be established by inverting multidisciplinary geophysical data constrained by geological and geostatistical priors. The method has been successfully proved by testing on a simple synthetic case. This synthetic case has highlighted the fact that quality of the results is improved using simultaneous inversion of independent fields.

The total litho-inversion method enables us to investigate the space of the possible 3D models compatible with the geological hypotheses (i.e., the a priori model) and with the geophysical and petrophysical data. This 3D inversion method applied to geological and geophysical data opens up new perspectives in terms of quantifying the geological uncertainties since given an a priori model it samples the space of solutions that satisfy the geophysical potential fields and tensors of these fields while respecting the surface geology, nature and topology of the geological units.

The generation of a space of solutions as a result of total litho-inversion is a concept that geologists should integrate in their approach to major scientific issues like the geometry of mountain belts or the coupling of deep-seated processes in the Earth and its surface. As far as it is stated that our capacity to predict the extension at depth of geological systems and units must be significantly improved, this integration process should be generalised.

Acknowledgments

Thank you all at Intrepid Geophysics (*3D GeoModeller* software distributor). We acknowledge Pr. Horst Holstein, for his comments and manuscript preparation.

References

Blanchin, R., Chilès, J.P., 1993. The Channel Tunnel: geostatistical prediction of the geological conditions and its validation by the reality. Math. Geol. 25, 963–974.
Bosch, M., Guillen, A., Ledru, P., 2001. Lithologic tomography: an application to geophysical data from the cadomian belt of northern Brittany, France. Tectonophysics 331, 197–228.
Calcagno, P., Courrioux, G., Guillen, A., Chilès, J.-P., this issue. Geological modelling from field data and geological knowledge. Part I. Modelling method coupling 3D potential-field interpolation and geological rules. Physics of the earth and planetary interiors.
Drinkwater, M.R., Floberghagen, R., Haagmans, R., Muzi, D., Popescu, A., 2003. GOCE: ESA's first Earth Explorer Core mission. In: Beutler, G.B., Drinkwater, M., Rummel, R., von Steiger, R. (Eds.), Earth Gravity Field from Space—from Sensors to Earth Sciences. In the Space Sciences Series of ISSI, vol. 18. Kluwer Academic Publishers, Dordrecht, Netherlands, pp. 419–432.
Faure, M., 1995. Late orogenic carboniferous extensions in the Variscan French Massif Central. Tectonics 14, 132–153.
Holstein, H., 2003. Gravimagnetic anomaly formulas for polyhedra of spatially linear media. Geophysics 68, 157–167.
Joly A., 2007. Relations plutons et discontinuités lithosphériques. Approche pluridisciplinaire de la mise en place de plutons granitiques le long du Sillon Houiller (Massif Central Français) - Thèse de doctorat de l'Université d'Orléans, 304 pp.
Joly, A., Martelet, G., Chen, Y., Faure, M., 2008. A multidisciplinary study of a syntectonic pluton close to a major lithospheric-scale fault—relationships between the Montmarault granitic massif and the Sillon Houiller Fault in the Variscan French Massif Central: 2. Gravity, aeromagnetic investigations, and 3-D geologic modeling. J. Geophys. Res. 113, B01404, doi:10.1029/2006JB004744.
Li, Y., Oldenburg, D., 1998. 3D inversion of gravity data. Geophysics 63, 109–119.
Metropolis, N., Ulam, S.M., 1949. The Monte Carlo method. J. Am. Stat. Assoc. 44, 335–341.
Metropolis, N., Rosenbluth, A.W., Rosenbluth, A.H., Teller, A.H., Teller, E., 1953. Equation of state calculations by fast computing machines. J. Chem. Phys. 1 (6), 1087–1092.
Mosegaard, K., Tarantola, A., 1995. Monte Carlo sampling of solutions to inverse problems. J. Geophys. Res. 100 (B7), 124321–212447.
Okabe, M., 1979. Analytical expressions for gravity anomalies due to homogeneous polyhedral bodies and translations into magnetic anomalies. Geophysics 44 (4), 730–741.
Pedersen, L.B., Rasmussen, T.M., 1990. The gradient tensor of potential field anomalies: some implications on data collection and data processing of maps. Geophysics 55 (12), 1558–1566.
Plouff, D., 1976. Gravity and magnetic fields of polygonal prisms and application to magnetic terrain corrections. Geophysics 41, 727–741.
Serra, J., 1982. Image Analysis and Mathematical Morphology, vol. 1. Academic Press.
Serra, J., 1988. Image Analysis and Mathematical Morphology, vol. 2. Academic Press.
Stadlober, E., Zechner, H., 1999. The patchwork rejection technique for sampling from unimodal distributions. ACM Trans. Model. Comput. Simul. 9 (1), 59–80.
Tarantola, A., 2005. Inverse problem theory and model parameter estimation. SIAM, 2005.
Tarantola, A., 2006. Popper, Bayes and the inverse problem. Nat. Phys. 2, 492–494.
Tarantola, A., Valette, B., 1982. Inverse problems = quest for information. J. Geophys. 50, 159–170.